Plasticized and Unplasticized PLA/Organoclay Nanocomposites: Short- and Long-Term Thermal Properties, Morphology, and Nonisothermal Crystallization Behavior

Serap Gumus,[1] Guralp Ozkoc,[1,2] Ayse Aytac[1]

[1]*Department of Chemical Engineering, Kocaeli University, Izmit, 41380, Kocaeli/Turkey*
[2]*Department of Polymer Science and Technology, Kocaeli University, Izmit, 41380, Kocaeli/Turkey*

Received 26 October 2010; accepted 29 April 2011
DOI 10.1002/app.34841
Published online 1 September 2011 in Wiley Online Library (wileyonlinelibrary.com).

ABSTRACT: The short- and long-term thermal properties, organoclay dispersion state, and the nonisothermal crystallization kinetics of organoclay based nanocomposites of poly(lactic acid) (PLA) and poly(ethylene glycol) (PEG) plasticized PLA were investigated. Differential scanning calorimetry analyses showed that plasticization of PLA/PEG blend was diminished due to physical aging by the time. The change in thermal properties such as glass transition temperature, cold crystallization temperature, and melting temperature was monitored. It was revealed from X-ray diffraction analyses that in long term, the exfoliated and/or intercalated organoclay structure of nanocomposites observed in short term (just after processing) was differentiated to a tactoidal form (i.e., nonseparated clays). The nonisothermal crystallization behavior and kinetics were examined by using Avrami, Ozawa, and combined Avrami–Ozawa models. Moreover, the nucleating effect of clays was investigated in terms of Gutzow and Dobrewa approaches. It was found out that clays did not act as nucleating agents in plasticized PLA nanocomposites, which was also in good agreement with activation energy values obtained from Kissinger and Takhor models. © 2011 Wiley Periodicals, Inc. J Appl Polym Sci 123: 2837–2848, 2012

Key words: PLA; nanocomposite; plasticization; physical aging; nonisothermal crystallization

INTRODUCTION

In recent years, researches in biodegradable polymers have attracted attention from packaging industry. A great quantity of petroleum based plastics is used for packaging purposes. As biodegradable polymers are produced from renewable sources, and easily composted into water and carbon dioxide, they are good alternatives to petroleum-based polymers.[1] The most popular biodegradable polymers are aliphatic polyesters, such as poly(lactic acid) (PLA), polycaprolactone (PCL), poly(butylene adipate terephthalate) (PBAT), and poly(hydroxy butyrate) (PHB).[2,3] Among them, PLA has a special place due to its high strength, high modulus, transparency, processability, and its commercially availability. An important requirement for packaging materials is high flexibility at room temperature.[3] However, the brittleness of PLA is a disadvantage to produce flexible films. Therefore, the flexibility of the PLA needs to be chemically or physically modified. Blending with plasticizers is a cost-effective physical modification method to improve flexibility.[4]

Plasticizers are used to decrease the glass transition temperature (T_g), increase the elongation at break and processability of polymers. A plasticizer should be compatible and miscible with the polymer matrix. Citrate ester, oligomeric lactic acid, poly(ethylene glycol) (PEG), and poly(propylene glycol) were reported to be compatible with PLA and used as effective plasticizers.[5] Miscibility of PLA/PEG blends has been extensively studied. It was found that blends up to 30 wt % PEG were miscible when they were quenched form the melt. They exhibited a single T_g and had no detectable crystallinity of either constituents.[6] However, the PLA plasticized with more than 30 wt % PEG was found to be unstable over the time and also an increase in modulus accompanied by a decrease in elongation at break was observed.[7,8] This was attributed to the migration and crystallization of PEG which results in phase separation in the blend. As a result, T_g increased due to the enriching of amorphous phase in PLA.[7]

For several years now, the field of polymer nanocomposites, especially layered silicates (clays), have received significant interest due to good physical performance of nano-scaled filler at a low loading level

Correspondence to: G. Ozkoc (guralp.ozkoc@kocaeli.edu.tr).

(1–5 wt %). Furthermore, it is known that fillers, such as clays, carbon nanotubes, calcium carbonate, and so on, may enhance the nucleation and the overall crystallization process by acting as nucleating agent during nonisothermal crystallization of semicrystalline polymers.[9–12] It is proved that the mechanical and physical properties of the crystalline polymers, such as PLA, depend on the supermolecular morphology that is controlled by the crystallization process in melt processing. Therefore, the kinetics of crystallization needs to be optimized to establish the structure–property correlations.

The crystallization behavior of neat PLA,[13–19] PLA stereocompleces,[20–22] and PLA/other polymer blends[23–26] has been investigated extensively by both isothermal and nonisothermal methods. The crystallization behavior of PLA-organoclay nanocomposites has also been studied to observe the effect of nanoclay on the properties of nanocomposites.[27] It was observed that the presence of clay increased the overall crystallization rate of PLA, but it did not have any effect on the crystal growth rate. The clay particles acted as a nucleating agent in PLA nanocomposites. This investigation was also confirmed by another study.[28] In the case of cold crystallization behavior, Pluta[29] found that PLA crystallized as a thin spherulitic structure during solid state quench process and, the presence of clay enhance the spherulite nucleation density and most probably disturb the organization of spherulites. The crystallization behavior of plasticized PLA nanocomposites was also investigated in an article. It was mentioned that plasticizer facilitated the crystallization process of both plasticized PLA and plasticized polymer matrix in nanocomposites.[28] However, there is no detailed study about nonisothermal crystallization kinetics of plasticized PLA/organoclay nanocomposites in the literature.

On the other hand, although plasticized PLA nanocomposites show good performance as a biodegradable material in short term, the phenomena so-called physical aging must be taken into consideration in determining the long-term properties. As a result of physical aging, the mechanical, optical, and barrier properties, and the crystallization behavior can change by the time (i.e., during storage period). Despite studies published on the physical aging of PLA and plasticized PLA,[6,8,30] there is not any study published in the literature focuses to the effects of physical aging on the nanoparticle dispersion and the thermal properties of plasticized PLA/organoclay nanocomposites.

The short-term properties of plasticized and unplasticized PLAs and their organoclay-based nanocomposites were investigated in our previous article.[31] In this study, the nonisothermal crystallization behavior of plasticized and unplasticized PLAs and their organoclay-based nanocomposites were studied by differential scanning calorimeter (DSC) adapting different crystallization models. Moreover, the long-term thermal properties and nanoclay dispersion were investigated by means of DSC and X-ray diffraction (XRD) analysis for the first time in the literature.

EXPERIMENTAL PROCEDURE

Materials

PLA (2002 D) was provided by NatureWorks Company, Nebraska/USA. Cloisite 30B, an organically modified montmorillonite (Southern Clay Products, Austin/USA), was used as the nanoclay filler because it was shown that Cloisite 30B/PLA nanocomposites exhibited intercalated or partially exfoliated structures.[31–34] The gallery spacing of this clay was reported as 1.85 nm.[31] PEG (1000 g/mol; Sigma-Aldrich, Istanbul/Turkey) was used as the plasticizer.

Sample preparation

PLA was dried for 12 h at 65°C, PEG and clay for 12 h at 35°C under vacuum before processing. PEG content was kept constant at 20% by weight in all compositions. Clay content was 0, 1, 3, and 5% by weight with respect to the matrix (PLA or PLA/PEG). The compounds were prepared in a co-rotating twin screw laboratory scale compounder (15 mL Microcompounder, DSM Xplore, Geleen/The Netherlands). This laboratory scale device can either be operated in continuous mode or in batch mode. To produce films, a cast film line (Micro film device, DSM Xplore, Geleen/The Netherlands) was connected to the laboratory scale compounder. The barrel temperature was 220°C, the screw speed was 100 rpm, and the residence time was 5 min. The process was conducted under nitrogen atmosphere. At the end of compounding, the compounder was shifted to force controlled mode from speed controlled mode to maintain a constant rate of throughput. A slit die with a thickness of 0.3 mm was used. To prevent necking and to fix the width, the film was cooled at the exit of the die by using an air-knife. The speed of collecting roller was arranged to obtain an average thickness of 0.25 ± 0.02 mm and width of 25 ± 2 mm film.

To examine the long-term properties, the films were stored at room temperature (relative humidity of 60% on average) for 1 year in polyethylene bags as wound on paper bobbins.

Characterization

XRD analysis

XRD analysis was conducted on nanocomposite films just after production for short-term investigation and after one year for long-term investigation by using a

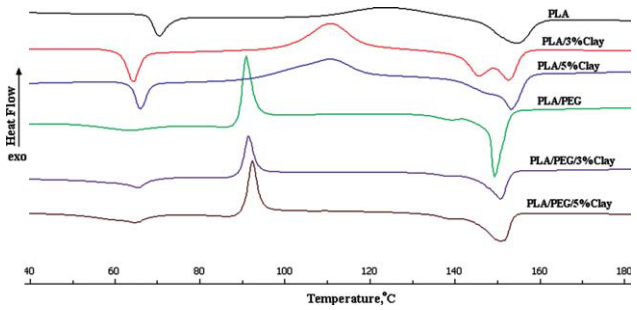

Figure 1 The first heating DSC-thermogram of plasticized and unplasticized PLA and their nanocomposites at a heating rate of 15°C/min [Color figure can be viewed in the online issue, which is available at wileyonlinelibrary.com.].

RIGAKU D/MAX 2200/PC XRD using X-ray source of Cu Kα (λ = 1.54 Å) radiation generated at a voltage of 40 kV and current of 40 mA. The diffraction angle 2Θ was scanned from 1° to 10° at a scanning rate of 0.5°/min.

Thermal properties

The short-term thermal properties were performed according to the procedure given elsewhere.[31] DSC (Metler Toledo DSC 1 Star System) analysis was performed to obtain long-term thermal properties. The films were heated from 25 to 180°C at a heating rate of 15°C/min.

To determine the transition temperatures, first derivative technique was used for the melting point, and second derivative technique was used for the glass transition temperature.

DSC analysis was performed to study the nonisothermal crystallization kinetics. The DSC procedure was consisting of three segments. At the first segment, the films were heated from 25 to 180°C with a heating rate of 15°C/min, then they were held at this temperature for 5 min to eliminate the thermal history, and then they were cooled to 25°C at cooling rates of 2, 5, 10, and 15°C/min and held at 25°C for 5 min. In the last segment, they were reheated to 180°C at a heating rate of 10°C/min.

RESULTS AND DISCUSSION

Short- and long-term thermal properties and nonisothermal crystallization kinetics

The long-term DSC thermograms of the PLA, PLA/PEG, and their nanocomposites obtained by heating samples from 25°C to 180°C with a heating rate of 15°C/min are given in Figure 1, and short- and long-term thermal transitions and degree of crystallinity values are given in Table I.

The common thermal characteristics of these materials are the glass transition temperature (T_g), the cold-crystallization temperatue (T_{cc}), and the melting temperature (T_{mc}). Moreover, there is also an endothermic peak that follows the T_g. This endothermic peak is due to the enthalpy relaxation during the physical aging.[35] As a result of quenching an amorphous polymer from higher temperature, that is, above the glass transition temperature (T_g) into the glassy state, the chain mobility decreases and the molecules cannot be able to reach an equilibrium packing density and conformational structure. In other words, molecules end up in a thermodynamically unequilibrium state. This phenomenon is called physical aging.[36,37] It is known that the glass transition temperature of PLA is about 60°C. During the film processing, the samples were rapid cooled by air below its glass transition temperature.[31] As a consequence, the molecular mobility was restricted, and the thermodynamically unstable state was reached. From this unstable state, the polymer chains rearranged slowly to reach the equilibrium during storage time.

The T_g of the plasticized PLA and plasticized PLA nanocomposites increased due to physical aging within one year (see Table I). This can be attributed to the phase separation of PLA and PEG as a consequence of rearrangement of PLA chains.[7] Besides, the peak of cold crystallization is shifted to higher values. As the degree of crystallinity of the aged and unaged samples are compared, no significant change observed as expected, because, the physical aging is a process related to the amorphous part of PLA.

TABLE I
The Characteristic Temperatures (°C) and Degree of Crystallinity (%) of PLA and its Nanocomposites at the First Heating Segment

Sample	Unaged samples[a]				Aged samples for one year			
	T_g	T_{cc}	T_{mc}	X_c	T_g	T_{cc}	T_{mc}	X_c
PLA	59.9	106	152.6	21.4	67.2	123.3	151.4	17.2
PLA/3%Clay	61.1	98.9	147.2	28.7	63.1	109.7	152.3	26.9
PLA/5%Clay	–	–	–	–	64.5	111.7	153.5	25.2
PLA/PEG	29.4	85.1	150.9	22.0	57.9	91.2	151.9	26.3
PLA/PEG/3%Clay	33.5	84.1	151.6	30.3	63.4	92.0	151.1	25.4
PLA/PEG/5%Clay	33.4	81.6	152.2	30.5	56.4	92.7	151.3	37.1

[a] This data was taken from our previous paper [31].

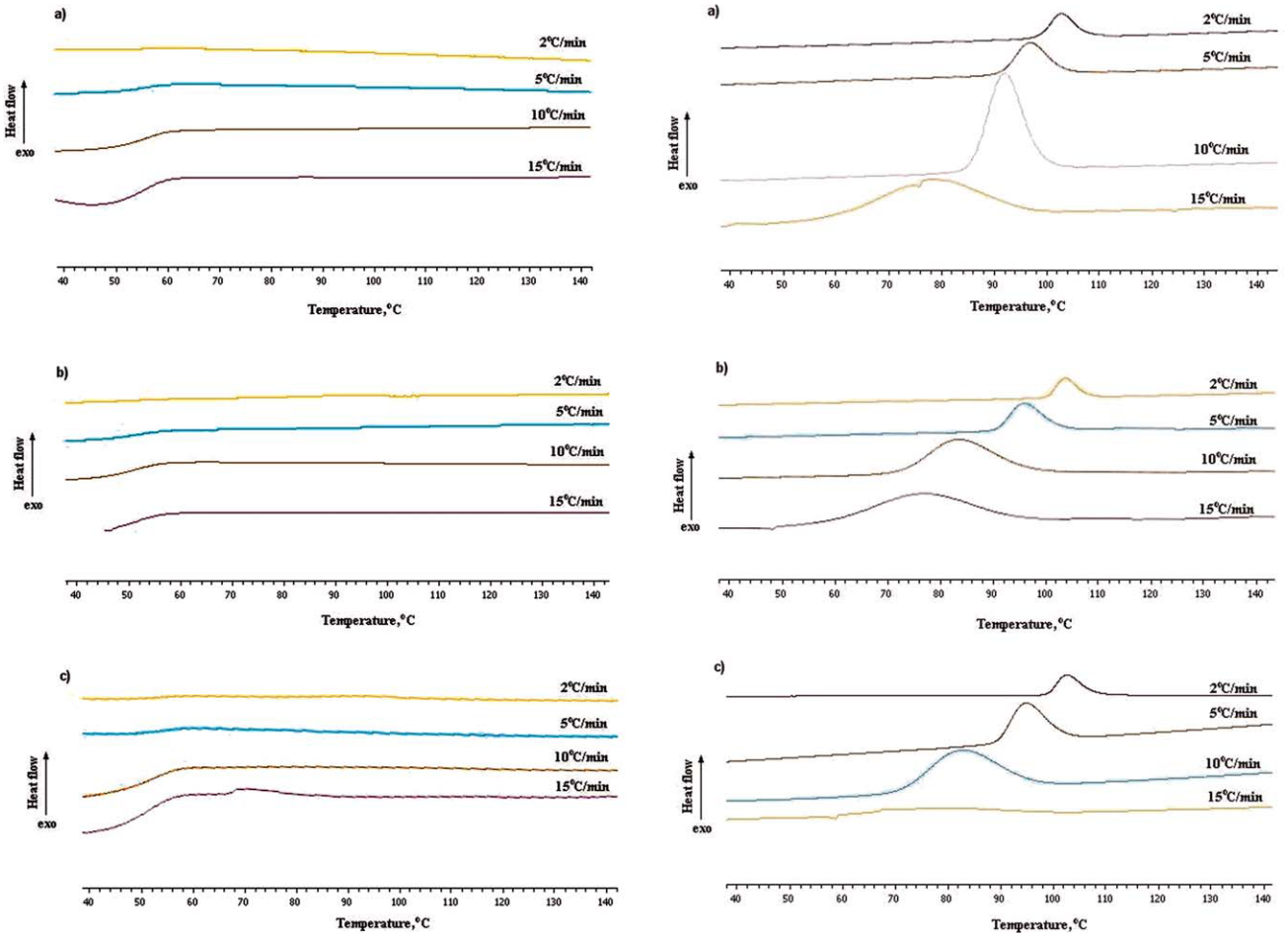

Figure 2 (i) The DSC thermograms of (a) PLA, (b) PLA/3%Clay, and (c) PLA/5%Clay at various cooling rates (see left column). (ii) The DSC thermograms of (a) PLA/PEG, (b) PLA/PEG/3%Clay, and (c) PLA/PEG/5%Clay at various cooling rates (see right column). [Color figure can be viewed in the online issue, which is available at wileyonlinelibrary.com.]

The analysis of nonisothermal crystallization kinetics could not be realized for nonplasticised PLA and its nanocomposites due to the formation of amorphous morphology during cooling process; however, plasticized films tend to crystallize in cooling. The nonisothermal crystallization thermograms of PLA/PEG, PLA/PEG/3%Clay, and PLA/PEG/5%Clay are given in Figure 2. The values of crystallization onset temperatures ($T_{c,\text{onset}}$), the peak temperatures ($T_{c,\text{peak}}$), the crystallization half time ($t_{1/2}$), the crystallization enthalpy (ΔH_c) calculated from DSC thermogram in cooling step, melting enthalpy (ΔH_m), and the degree of crystallinity (X_c) obtained from the second heating step are given in Table II. For all samples, the crystallization peak becomes wider and shifted to lower temperature by increasing the cooling rate. It means that at lower cooling rates, most of semicrystalline polymers spent longer time within the temperature range that promote sufficient mobility of segments for the growth of crystallization.[38] In other words, more supercooling was required to initiate crystallization, because the motion of the polymer molecules could not follow the cooling rate when the samples cooled rapidly from the melt.[39] Addition of clay to the plasticized PLA does not affect the $T_{m,\text{onset}}$ at low cooling rates such as 2°C/min and 5°C/min; however, at higher cooling rates, the $T_{c,\ \text{onset}}$ of PLA/PEG is higher than that of the plasticized PLA nanocomposites. Furthermore, if the cooling rate is too high, there will not be enough time to a conformational arrangement for the chains to go into crystalline state; therefore, it will be totally amorphous. Addition of potential nucleating agents, that is, nanoclays[40,41] is also found to be ineffective in crystallization process. This phenomenon was explained by Krikorian and Pochan.[42,43] Cloisite 30B, an organically modified montmorillonite, is a compatible organoclay with PEG plasticised PLA matrix. Due to the interfacial energy between the matrix and the modifier used in Cloisite 30B, the dispersed clay platelets hinder the chain-folding which is needed for the local PLA crystallization. This means that highly compatible clays with the matrix hinder the interchain interactions necessary for crystal nuclei formation.

At slow cooling rates, the crystallization onset temperatures of matrix and nanocomposites found

TABLE II
The Characteristic Properties of Plasticized PLA and its Nanocomposites Obtained at Different Cooling Rates

Sample	β (C/min)	$T_{c,onset}$ (°C)	$T_{c,\ peak}$ (°C)	$t_{1/2}$ (min)	ΔH_c (J/g)	ΔH_m (J/g)	X_c (%)
PLA/PEG	2	107.09	102.26	3.26	22.08	22.42	30.1
	5	102.84	96.54	1.82	22.0	23.56	31.7
	10	99.01	91.76	1.31	21.98	23.02	30.9
	15	96.91	77.56	1.11	18.07	29.74	39.9
PLA/PEG/ 3%Clay	2	107.51	103.44	3.29	21.78	24.36	34.0
	5	102.32	95.63	2.29	19.05	22.74	31.7
	10	96.20	83.57	1.83	22.29	30.42	42.5
	15	93.66	76.54	1.67	12.89	26.46	36.9
PLA/PEG/ 5%Clay	2	107.28	102.54	3.24	27.70	31.47	45.1
	5	102.07	94.83	2.27	22.80	24.65	35.3
	10	95.50	82.57	1.74	18.45	25.46	36.5
	15	–	–	–	–	24.95	35.8

to be the same; however, at higher cooling rates, the crystallization onset temperature was suppressed for PLA/PEG matrix in comparison with their nanocomposites. This is due to the lack of time for a new arrangement to go into the crystalline state. To determine the crystallization rate, the relative crystallinity can be plotted as a function of either temperature or time. Equation (1) shows the relative crystallinity, $X(T)$, versus crystallization temperature.

$$X(T) = \int_{T_0}^{T} \left(\frac{dH_c}{dT}\right) dT \Big/ \int_{T_0}^{T_\infty} \left(\frac{dH_c}{dT}\right) \cdot dT \qquad (1)$$

where T_0 and T_∞ are the onset and the endset temperatures of the crystallization process, respectively; T is any temperature in crystallization process and dH_c represents the differential crystallization enthalpy change in temperature range of dT.

Figure 3 shows the dependence of relative crystallinity with respect to temperature. All plots indicate a sigmoidal shape. At the beginning of the crystallization process, the first plateau of the curves is the induction period where the nucleations are formed. At the end of the nucleation stage, the crystallites begin to grow. This is the accelerated crystallization period, which can be seen from the descending linear second part. This accelerated crystallization period continues until the crystallites begin to touch each other. By touching each other, the crystallization rate decreases, but the crystallinity still increases slowly. This action is distinguished by the deviated part of the curve and referred to secondary crystallization.[44–46]

Crystallization time, t, can be obtained from eq. (2):

$$t = (T_0 - T)/\beta \qquad (2)$$

where T is the temperature at the crystallization time t and β is the cooling rate. This equation can be used to evaluate the relationship between the relative crystallization ($X(t)$) and the crystallization time (t). Moreover, the crystallization half time $t_{1/2}$ which is the required time to reach the 50% of relative crystallinity can be calculated. $X(t)$ versus time plots are represented in Figure 4. The higher the cooling rate, the shorter the time required for crystallization process. Addition of clay to plasticized PLA does not significantly affect the rate of crystallization.

Generally, Avrami model is used to explain the isothermal crystallization behavior of semicrystalline polymers.[47–49] Nucleation and crystal growth processes in nonisothermal crystallization dependent on the temperature, that is, rate of cooling. However, Avrami Model can be applied to the linear part of the curves (Fig. 5), which describes the primary stage of nonisothermal crystallization. The Avrami equation is given as follows:

$$1 - X(t) = \exp(-Zt^n) \qquad (3)$$

where $X(t)$ is the relative degree of crystallinity at time t, Z is the rate constant giving the information about the nucleation and the growth rate. The Avrami exponent "n" gives information about the nucleation type and the morphology of the crystallite formed. The double logarithm of the eq. (3) is usually taken to calculate the rate constant Z and the Avrami exponent n [eq. (4)].

$$\ln(-\ln(1 - X(t))) = \ln Z + n \cdot \ln t \qquad (4)$$

From the plot of $\ln(-\ln(1 - X(t))$ versus $\ln t$, the slope and the intercept will give n and Z, respectively. Avrami equation is generally applied to isothermal conditions. Jeziorny[50] revised the crystallization rate Z in Avrami equation by dividing with cooling rate β to incorporate the temperature change during the nonisothermal crystallization process as follows:

$$\ln Z_C = \frac{\ln Z}{\beta} \qquad (5)$$

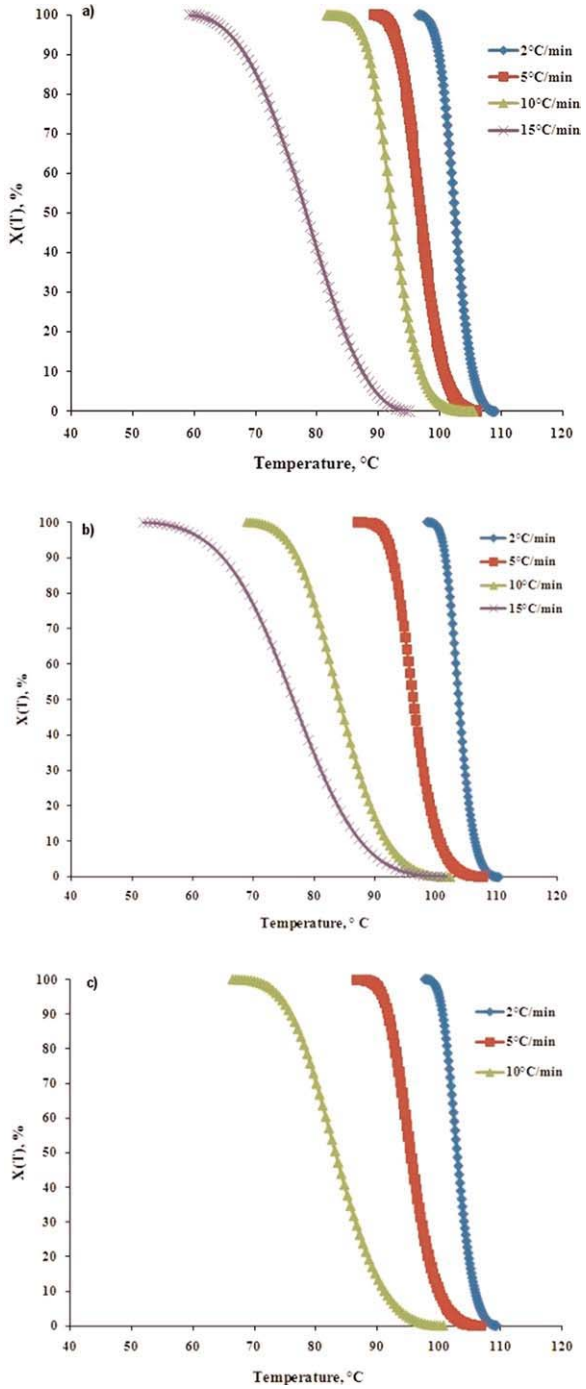

Figure 3 Relative crystallinity, $X(T)$, as a function of temperature at different cooling rates (a) PLA/PEG, (b) PLA/PEG/3%Clay, and (c) PLA/PEG/5%Clay [Color figure can be viewed in the online issue, which is available at wileyonlinelibrary.com.].

The Avrami plots are given in Figure 5. The curves consist of two parts with different slopes. These two parts correspond to the two crystallization stage, namely the primary and secondary crystallization, respectively. Primary crystallization is the macroscopic development of the degree of crystallinity as a result of nucleation and subsequent crystal growth.[44] Secondary crystallization is the further slower crystallization and perfection of initially crystallized macromolecules after the primary crystallization is over. The secondary crystallization can be

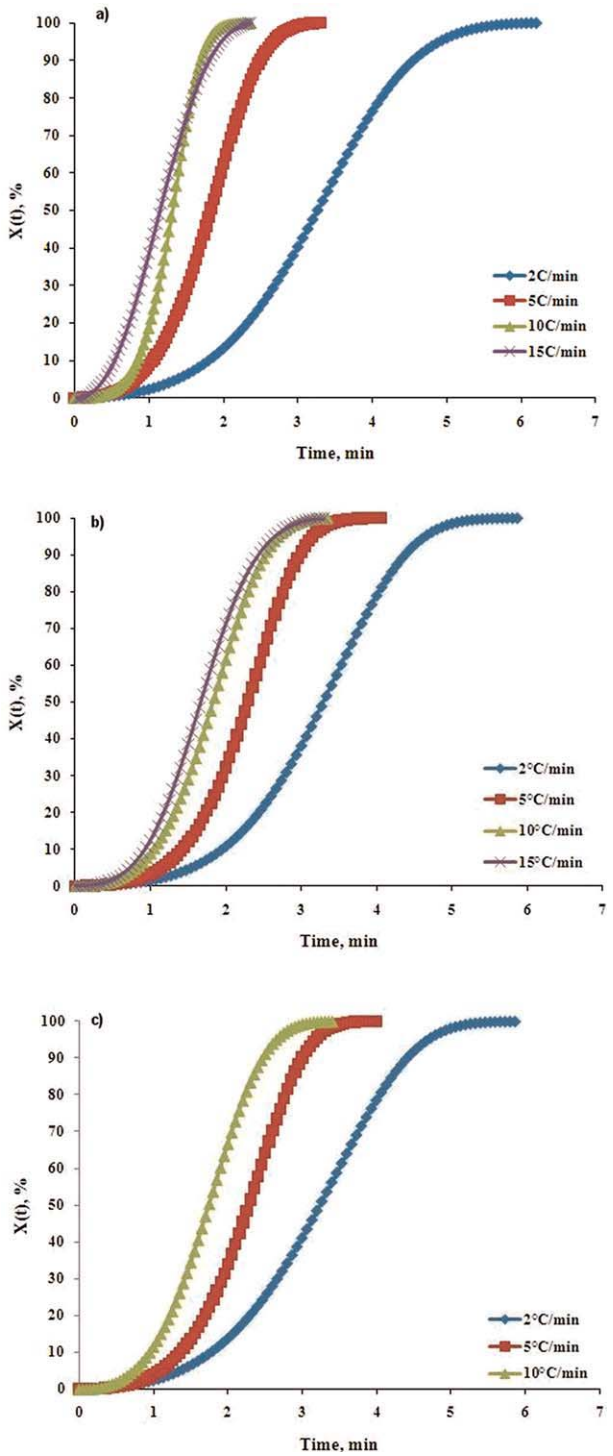

Figure 4 Relative crystallinity, $X(t)$, as a function of time at differetnt cooling rates (a) PLA/PEG, (b) PLA/PEG/3%Clay, and (c) PLA/PEG/3%Clay [Color figure can be viewed in the online issue, which is available at wileyonlinelibrary.com.].

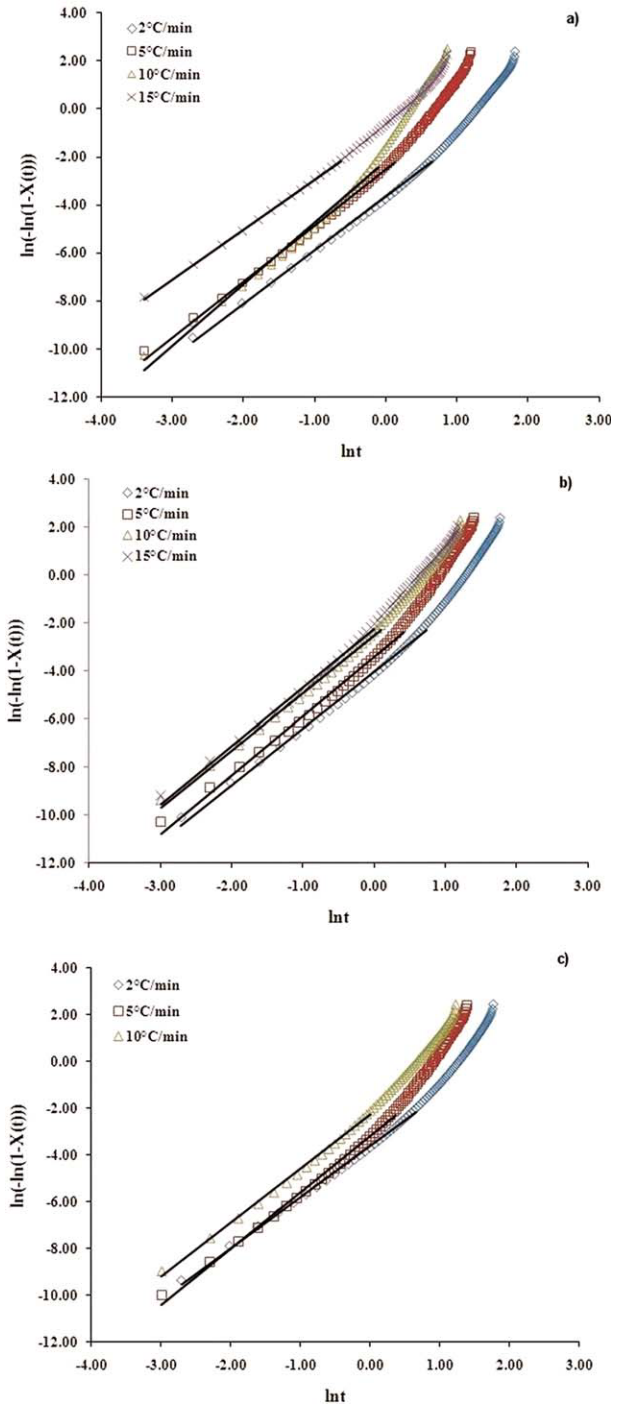

Figure 5 Avrami plots of the samples (a) PLA/PEG, (b) PLA/PEG/3%Clay, and (c) PLA/PEG/3%Clay [Color figure can be viewed in the online issue, which is available at wileyonlinelibrary.com.].

identified by the deviation from the linear part of the curve of Avrami plots. The slope of the deviated part is smaller due to the decreased crystallization rate. Primary crystallization which is describable by Avrami equation can be examined by using the part of the curve given in Figure 5, in which $\ln(-\ln(1 - X(t)) < 0$. The calculated values of the rate constant Z_c and the Avrami exponent n are given in Table III.

The values of n for plasticized PLA and its nanocomposites are around 2. This value points out that the primary crystallization of the samples can either be two-dimensional (2D), circular crystal growth with an athermal nucleation or 2D, circular diffusion controlled crystal growth with a thermal nucleation.[51,52] The rate constant Z_c increased with increasing cooling rate for all of the samples meaning that the crystallization rate is higher and the melt crystallization takes place at lower temperatures. Besides, the Z_c value is decreased by adding clay to plasticized PLA at a given cooling rate. The same trend is seen by comparing the crystallization half time values.

Another approach for the nonisothermal crystallization kinetic is the Ozawa model.[53] The effect of cooling rate and the temperature variation with time is not considered in Avrami model, whereas nonisothermal crystallization is effected by cooling rate. The modified Avrami model by Ozawa is given as follows:

$$\ln(-\ln(1 - X(t))) = \ln K(t) - m \cdot \ln \beta \qquad (6)$$

where $K(T)$ represents the cooling function and "m" is the Ozawa exponent. The Ozawa plot for plasticized PLA and its nanocomposites are shown in Figure 6. As can be seen, the Ozawa model is failed to describe the nonisothermal crystallization for this case. If the Ozawa model were suitable, the slope of parallel lines and $K(T)$ value for each temperature would be negative. Because of the different cooling rates, the crystallization process occurs in different temperature intervals; therefore, the crystallization stage will be different from each other at a given temperature and cooling rate.

Mo et al. proposed a different kinetic approach to describe a nonisothermal process by combining Avrami and Ozawa equation at a given $X(t)$ as follows [eqs. (7) and (8)][54]:

TABLE III
Avrami Kinetic Parameters at Different Cooling Rates

Sample	β (C/min)	n	Z	Z_c	R^2
PLA/PEG	2	2.23	0.02	0.16	0.998
	5	2.33	0.08	0.60	0.995
	10	2.56	0.11	0.80	0.986
	15	2.07	0.42	0.94	0.998
PLA/PEG/3%Clay	2	2.37	0.02	0.13	0.995
	5	2.46	0.03	0.51	0.991
	10	2.39	0.08	0.78	0.996
	15	2.43	0.11	0.86	0.995
PLA/PEG/5%Clay	2	2.18	0.03	0.16	0.997
	5	2.40	0.04	0.53	0.995
	10	2.31	0.10	0.79	0.997
	15	–	–	–	–

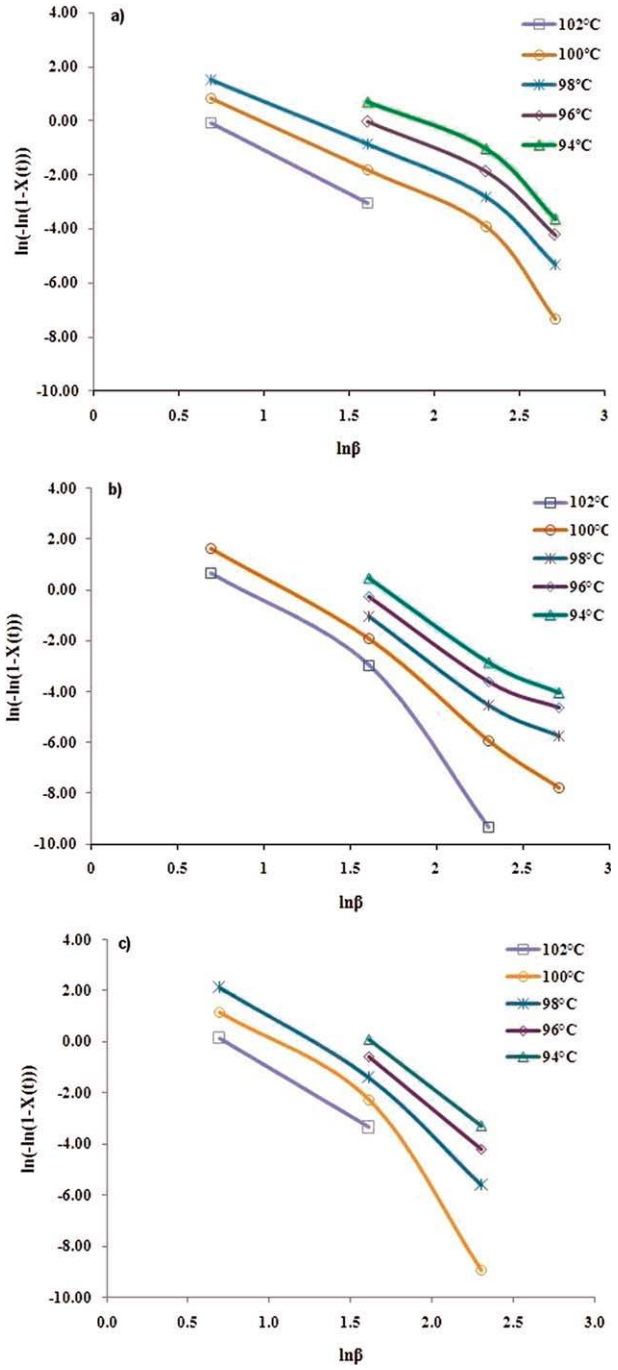

Figure 6 Ozawa plots of the samples (a) PLA/PEG, (b) PLA/PEG/3%Clay, and (c) PLA/PEG/3%Clay [Color figure can be viewed in the online issue, which is available at wileyonlinelibrary.com.].

$$\ln Z + n \cdot \ln t = \ln K(T) - m \cdot \ln \beta \quad (7)$$

$$\ln \beta = \ln F(T) - \alpha \cdot \ln t \quad (8)$$

The kinetic parameter $F(T) = [K(T)/Z]^{\frac{1}{m}}$ is the required cooling rate to reach a certain degree of crystallinity at a unit time. Therefore, high $F(T)$ values mean higher cooling rates that are needed to reach the certain value of relative crystallinity in the unit time, α is equal to the ratio of the Avrami exponent n to the Ozawa exponent m. The slope gives the value of α and the intercept gives the kinetic parameter $F(T)$ by plotting $\ln\beta$ against $\ln t$. Figure 7 shows the plots of plasticized PLA and its nanocomposites at different relative crystallinity values. The

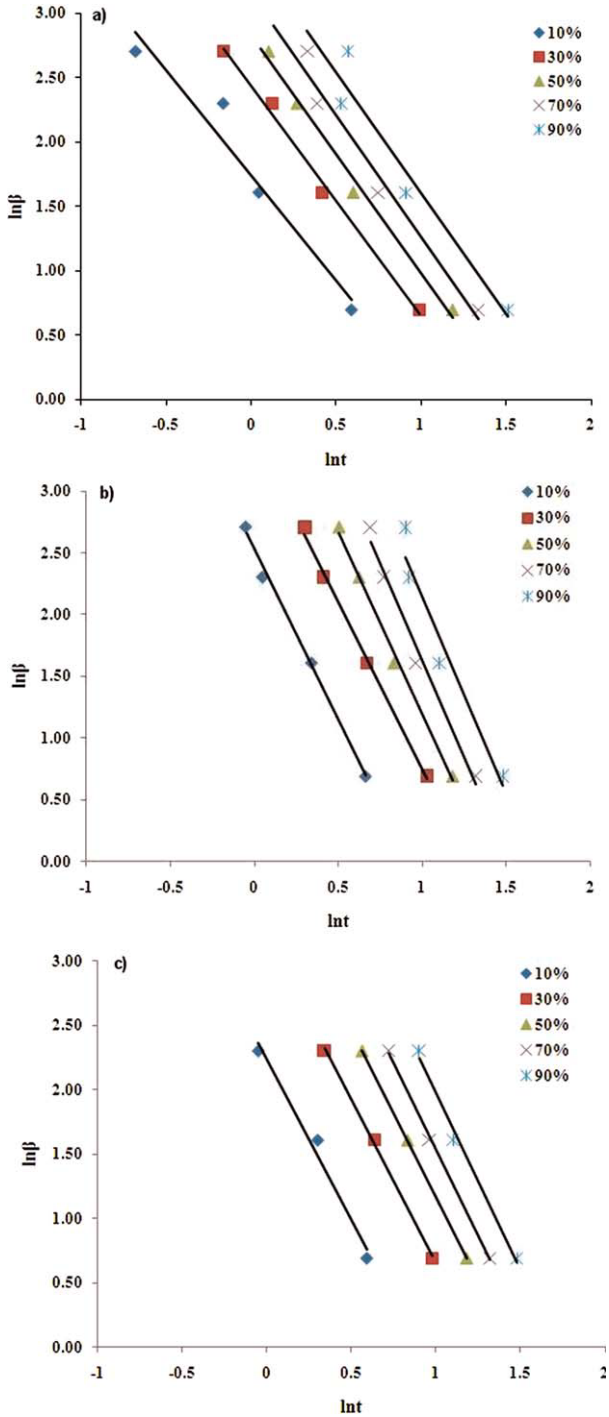

Figure 7 Combined Ozawa and Avrami model plots of the samples (a) PLA/PEG, (b) PLA/PEG/3%Clay, and (c) PLA/PEG/3%Clay [Color figure can be viewed in the online issue, which is available at wileyonlinelibrary.com.].

TABLE IV
The Calculated Kinetic Parameters at Different Cooling Rates Obtained from Combined Ozawa and Avrami Model

Sample	$X(t)$ (%)	α	$F(T)$	Activation energy from Kissinger (kJ/mol)	Activation energy from Takhor (kJ/mol)
PLA/PEG	10	1.64	5.69	−87.24	−81.31
	30	1.79	11.47		
	50	1.85	16.94		
	70	1.88	23.34		
	90	1.88	32.78		
PLA/PEG/3%Clay	10	2.76	12.43	−86.07	−79.91
	30	2.71	31.82		
	50	2.95	62.80		
	70	3.12	114.43		
	90	3.19	208.51		
PLA/PEG/5%Clay	10	2.49	9.29	−93.29	−87.22
	30	2.52	24.05		
	50	2.59	42.95		
	70	2.67	67.36		
	90	2.73	108.85		

values of the kinetic parameters obtained from the plots are given in Table IV.

The α values increased by increasing the relative crystallinity for all the samples. However, α value of plasticized PLA is smaller than that of plasticized PLA nanocomposites. The values of kinetic parameter $F(T)$ exhibits similar trend to the values of α. $F(T)$ increases with relative crystallinity and addition of clay at a given crystallinity degree. This means that addition of clay to plasticized PLA need higher rate of cooling to reach a certain crystallinity degree at unit time. In other words, the crystallization rate of plasticized PLA nanocomposites is lower than that of plasticized PLA. This is also in good agreement with the results obtained from crystallization half time and Avrami analysis.

Addition of reinforcing fillers in polymers can enhance its mechanical properties and thermal stability.[29] Furthermore in many case, the substrates such as clays act as nucleating agents[40,41]; therefore, the magnitude of the effect of nucleating activity should be measured. Dobreva and Gutzow[9,55,56] suggest a simple method to measure the effect as nucleating agent, so-called nucleating activity, φ, as follows:

$$\varphi = \frac{B^*}{B} \tag{9}$$

where B^* and B are the parameters of heterogeneous and homogeneous medium, respectively. If the additive does not act as a nucleating agent, the value of φ will be unity; on the other hand, it approaches to zero, if it acts as a nucleating agent. B parameter is defined as:

$$B = \frac{\omega\sigma^3 V_m^2}{3nk_B T_m^0 \Delta S_m^2} \tag{10}$$

where ω is the geometric factor, σ is the specific energy. V_m is the molar volume of the crystallizing substance, n is the Avrami exponent, k_B is the Boltzmann constant, ΔS_m is the melting entropy, and T_m^0 is the equilibrium melting temperature. Furthermore, the B parameter can be obtained from experimental values using the equation given below:

$$\ln\beta = C - \frac{B}{\Delta T_c^2} \tag{11}$$

where, β is the cooling rate, C is a constant and ΔT_c is the supercooling (T_m-T_c). From eq. (11), the B and B^* parameters can be calculated by plotting lnβ versus $1/\Delta T_c^2$. The slope will give the B for plasticized PLA and B^* for plasticized PLA nanocomposites.

The plots for the plasticized PLA and its nanocomposites are given in Figure 8. The B parameter for plasticized PLA is calculated as 7693, whereas B^* parameter for plasticized nanocomposites with 3% clay and 5% clay are 7102 and 7332, respectively.

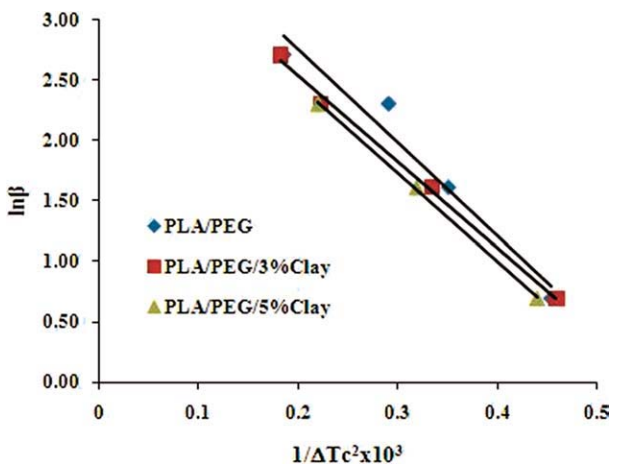

Figure 8 Nucleation activity plots of the samples [Color figure can be viewed in the online issue, which is available at wileyonlinelibrary.com.].

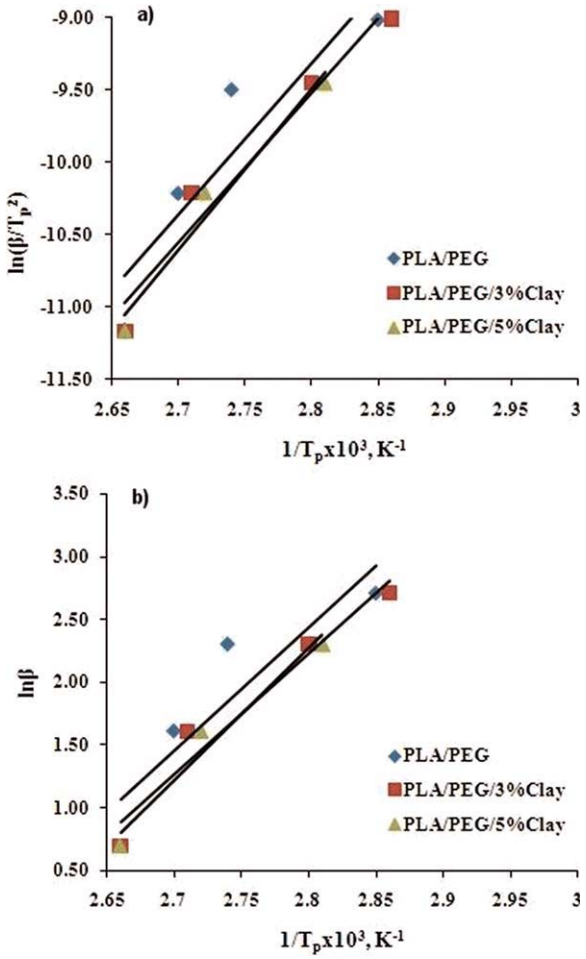

Figure 9 Activation energy of melt crystallization of the samples calculated from (a) Kissinger and (b) Takhor approaches [Color figure can be viewed in the online issue, which is available at wileyonlinelibrary.com.].

The corresponding B^*/B values are 0.92 and 0.95 for 3 and 5% clay incorporated plasticized PLA, respectively. These values indicate that clay does not behave as a nucleating agent.

There are many mathematical approaches to evaluate the activation energy (ΔE) of the crystallization process. The approach proposed by Kissinger[9,57] and Takhor[41,58] are used in this study. The equation of Kissinger and Takhor are given in eqs. (12) and (13), respectively:

$$\frac{d\left[\ln\left(\frac{\beta}{T_p^2}\right)\right]}{d\left(\frac{1}{T_p}\right)} = -\frac{\Delta E}{R} \tag{12}$$

$$\frac{d(\ln \beta)}{d\left(\frac{1}{T_p}\right)} = -\frac{\Delta E}{R} \tag{13}$$

where T_p is the peak temperature, β is the cooling rate, and R is the universal gas constant. The calculated values of activation energy (Fig. 9) are given in Table IV. It can be concluded that the activation energies obtained from Kissinger and Takhor approaches are not affected by the presence of clay. Therefore, it is proven once again that clays do not play the role of nucleating agent.

XRD analysis: Short- and long-term nanoparticle dispersion

The XRD analysis was performed to observe the nano scale dispersion of clays in the polymer matrix by monitoring the changes in the basal spacing (d-spacing). The clay used in this study is an organically modified montmorillonite (Cloisite 30B). The detailed properties and the XRD pattern of neat Cloisite 30B were given in our previous article.[15] The peak giving the basal spacing of Cloisite 30B is seen around $2\Theta = 5^\circ$, which corresponds to a d-spacing of 18 Å. It is known that several clay-polymer morphology in nanocomposites can be obtained as a function of processing conditions and organoclay-polymer compatibility. A complete separation of clay platelets due to a high compatibility between organoclay and polymer, and enough shear stress during processing is called exfoliation, which is the most preferred morphology in polymer nanocomposites.[59] Figure 10 shows the change of the clay distribution in PLA and plasticized PLA at the end of aging process. In unplasticized nanocomposites of PLA/3%Clay, the peaks indicating an intercalated/tactoidal morphology appeared at $2\theta \cong 2^\circ$ and $2\theta \cong 5^\circ$ became sharper by aging; whereas, the almost fully exfoliated structure in the plasticized nanocomposite (PLA/PEG/3%Clay) is turned into a partially intercalated structure. This indicates that during the physical aging, the intercalated clay platelets tend to return to their initial, nonseparated (neither intercalated nor exfoliated) structure. Concerning the competition between PLA chains and PEG molecules in the intercalation process, it was concluded in our previous study that PEG was preferentially diffuses through the clay galleries in comparison with PLA due to its smaller molecular dimensions by acting as an exfoliation promoter.[15] Due to the rearrangement and phase separation process during aging, PEG diffused out of clay galleries which results in aggregation of clay platelets.

CONCLUSIONS

A comparison of short- and long-term thermal properties and dispersion of organoclay based nanocomposites of PLA and plasticized PLA were performed. In addition to that, the nonisothermal crystallization behavior was investigated by using different kinetic models. In long term, the T_g and T_{cc} of plasticized PLA and their nanocomposites increased; however, T_{mc} and $\%X_c$ remained unchanged. The Avrami

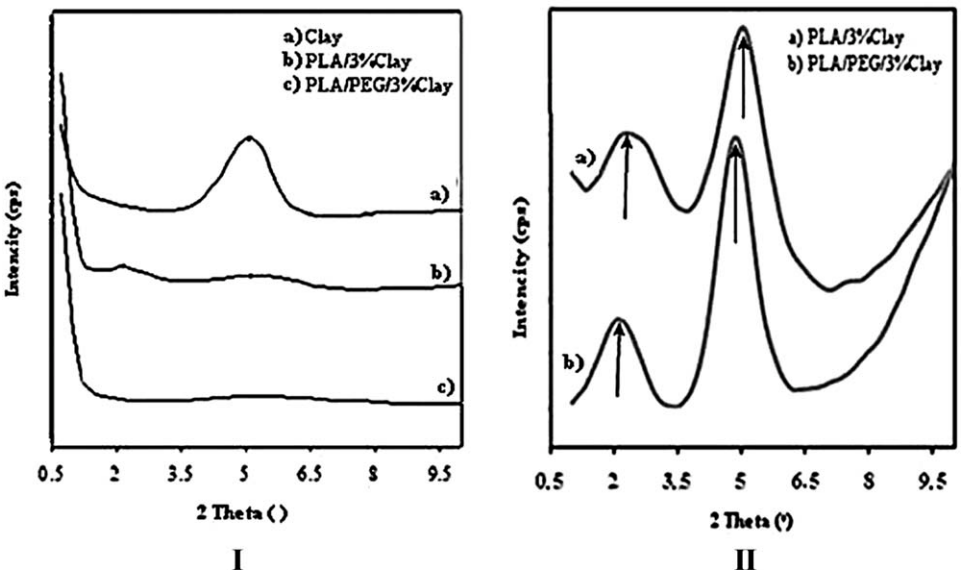

Figure 10 Comparison of diffractograms of (I) Unaged PLA and PLA/PEG nanocomposites: (a) Clay (Cloisite 30®B), (b) PLA/3%Clay, and (c) PLA/PEG/3%Clay and (II) Aged PLA and PLA/PEG nanocomposites: (a) PLA/3%Clay and (b) PLA/PEG/3%Clay.

based kinetic analysis pointed out that the primary crystallization of the samples can either be 2D, circular crystal growth with an athermal nucleation or 2D, circular diffusion controlled crystal growth with a thermal nucleation. Ozawa based kinetic analysis was failed to describe the nonisothermal crystallization of plasticized PLA and its nanocomposites. The combined Ozawa and Avrami model results were in well agreement with the results obtained from crystallization half time and Avrami analysis. Moreover the simple method suggested by Dobreva and Gutzow showed that organoclay did not act as nucleation agent in plasticized PLA. The activation energy of the nonisothermal crystallization is calculated by using Kissinger and Takhor. The values obtained for matrix and its clay based nanocomposites were similar to each other, which also supported that the clays did not play the role as a nucleating agent. XRD analyses showed that the intercalated and/or exfoliated clays turned to tactoids as a result of physical aging of PLA and migration and phase separation of PEG within 1 year of aging period.

References

1. Su, X. S. In Bio-Based Polymers and Composites; Wool, R. P.; Su, X. S., Eds.; Elsevier Science & Technology Books: UK, 2005; Chapter 1, pp 1.
2. Demirbaş, A. Energy Sourc Part A 2007, 29, 419.
3. Pillin, I.; Montrelay, N.; Grohens, Y. Polymer 2006, 47, 4676.
4. Ljungberg, N.; Wesslen, B. Biomacromolecules 2005, 6, 1789.
5. Wang, R.; Wan, C.; Wang, S.; Zhang, Y. Polym Eng Sci 2009, 49, 2414.
6. Hu, Y.; Rogunova, M.; Topolkaraev, V.; Hiltner, A; Baer, E. Polymer 2003, 44, 5701.
7. Ljungberg, N.; Wesslen, B. Polymer 2003, 44, 7679.
8. Hu, Y.; Hu, Y. S.; Topolkaraev, V; Hiltner, A.; Baer, E. Polymer 2003, 44, 5711.
9. Durmuş, A.; Ercan, N.; Soyubol, G.; Deligöz, H.; Kaşgöz, A. Polym Compos 2010, 31, 1056.
10. Di Lorenzo, M. L. Eur Polym J 2005, 41, 569.
11. Miyata, T.; Masuko, T. Polymer 1998, 39, 5515.
12. He, Y.; Fan, Z. Y.; Hu, Y. F.; Wu, T.; Wei, J.; Li, S. M. Eur Polym J 2007, 43, 4431.
13. Kalb, B.; Pennings, A. J. Polymer 1980, 21, 607.
14. Carla, M.; Antonio, M.; Vito, D. N. Macromol Chem 1992, 193, 1599.
15. Cartier, L.; Okihara, T.; Ikada, Y.; Tsuji, H.; Puiggali, J.; Lotz, B. Polymer 2000, 41, 8909.
16. Mano, J. F.; Wang, Y. M.; Viana, J. C.; Denchev, Z.; Oliveira, M. J Macromol Mater Eng 2004, 289, 910.
17. Zhang, J. M.; Tsuji, H.; Noda, I.; Ozaki, Y. Macromolecules 2004, 37, 6433.
18. Miyata, T.; Masuko, T. Polymer 1997, 38, 4003.
19. Urayama, H.; Kanamori, T.; Fukushima, K.; Kimura, Y. Polymer 2003, 44, 5635.
20. Schimidt, S. C.; Hillmyer, M. A. J Polym Sci Part B: Polym Phys 2001, 39, 300.
21. Tsuji, H.; Tezuka, Y. Biomacromolecules 2004, 5, 1181.
22. Sarasua, J. M.; Rodriguez, N. L.; Arraiza, A. L.; Meaurio, E. Macromolecules 2005, 38, 8362.
23. Nam, J. Y.; Okamoto, M.; Okamoto, H.; Nakano, M.; Usuki, A.; Matsuda, M. Polymer 2006, 47, 1340.
24. Liu, T. Y.; Lin, W. C.; Yang, M. C.; Chen, S. Y. Polymer 2005, 46, 12586.
25. Furukawa, T.; Sato, H.; Murakami, R.; Zhang, J.M.; Noda, I.; Ochiai, S.; Ozaki, Y. Polymer 2006, 47, 3132.
26. Jiang, L.; Wolcott, M. P.; Zhang, J. W. Biomacromolecules 2006, 7, 199.
27. Nam, J. Y.; Ray, S. S.; Okamoto, M. Macromolecules 2003, 36, 7126.
28. Pluta, M. Polymer 2004, 45, 8239.
29. Pluta, M.; Galeski, A.; Alexandre, M.; Paul, M. A. Dubois, P. J Appl Polym Sci 2002, 86, 1497.
30. Pluta, M.; Paul, M. A.; Alexandre, M.; Dubois, P. J Polym Sci Part B: Polym Phys 2006, 44, 312.
31. Ozkoc, G.; Kemaloglu, S. J Appl Polym Sci 2009, 144, 2481.

32. Paul, M. A.; Alexandre, M.; Degee, P.; Henrist, C.; Rulmont, A.; Dubois. P. Polymer 2005, 44, 443.
33. Krikorian, V.; Pochan, D. J. Chem Mater 2003, 15, 4317.
34. Lee, S.Y.; Hana, M. A. Polym Compos 2009, 30, 665.
35. Pan, P.; Zhu, B.; Inoue, Y. Macromolecules 2007, 40, 9664.
36. Hutchinson, J. M. Prog Polym Sci 1995, 20, 703.
37. Struik, L. C. E. Polym Eng Sci 1977, 17, 165.
38. Zhang, C.; Zhu, B.; Ji, G.; Xu, Y. J. Appl Polym Sci 2006, 99, 2782.
39. Yang, G.; Chen, X.; Wang, W.; Wang, M.; Liu, T.; Li, C. J. Polym Sci Part B: Polym Phys 2007, 45, 976.
40. Ray, S. S.; Okamoto, M. Macromol Rapid Commun 2003, 24, 815.
41. Wang, Y.; Shen, C.; Li, H.; Li, Q.; Chen, J. J Appl Polym Sci 2004, 91, 308.
42. Krikorian, V.; Pochan D. J. Macromolecules 2004, 37, 6480.
43. Krikorian, V.; Pochan D. J. Macromolecules 2005, 38, 6520.
44. Ren, M.; Song, J.; Zhao, Q.; Li, Y.; Chen, Q.; Zhang, H.; Mo, Z. Polym Int 2004, 53, 1658.
45. Papageorgiou, G. Z.; Achilias, D. S.; Bikiaris, D. N.; Karayannidis, G. P. Thermochim Acta 2005, 427, 117.
46. Su, Z.; Guo, W.; Liu, Y. Polym Bull 2009, 62, 629.
47. Avrami, M. J Chem Phys 1939, 7, 1103.
48. Avrami, M. J Chem Phys 1940, 8, 212.
49. Avrami, M. J Chem Phys 1941, 9, 177.
50. Jeziorny, A. Polymer 1978, 19, 1142.
51. Wunderlich, B. Macromolecular Physics; Academic Press: UK, 1976; Vol.2. Chapter 6, pp 146–147.
52. Wu, D.; Wu, L.; Wu, L.; Xu, B.; Zhang, Y.; Zhang, M. J Polym Sci Part B: Polym Phys 2007, 45, 1100.
53. Ozawa, T. Polymer 1971, 12, 150.
54. Liu, T.; Mo, Z.; Wang, S.; Zhang, H. Polym Eng Sci 1997, 37, 568.
55. Dobreva, A; Gutzow, I. J Non-Cryst Solids 1993, 162, 1.
56. Dobreva, A; Gutzow, I. J Non-Cryst Solids 1993, 162, 13.
57. Kissinger, H. E. J Res Natl Bur Stand 1956, 57, 217.
58. Takhor, R.L. Advances in Nucleation and Crystallization of Glasses; American Ceramics Society: Columbus. OH, 1971, pp 166–172.
59. Dennis, H. R.; Hunter, D. L.; Chang, D.; Kim, S.; White, J. L.; Cho, J. W.; Paul, D.R. Polymer 2001, 42, 9513.